---

**Article:**
Vasilev, C. orcid.org/0000-0002-0536-882X, Swainsbury, D.J.K. orcid.org/0000-0002-0754-0363, Cartron, M.L. et al. (6 more authors) (2022) FRET measurement of cytochrome bc1 and reaction centre complex proximity in live Rhodobacter sphaeroides cells. Biochimica et Biophysica Acta (BBA) - Bioenergetics, 1863 (2). 148508. ISSN 0005-2728

https://doi.org/10.1016/j.bbabio.2021.148508

---

# FRET measurement of cytochrome *bc*$_1$ and reaction centre complex proximity in live *Rhodobacter sphaeroides* cells

Cvetelin Vasilev[1]*, David J.K. Swainsbury[1], Michael L. Cartron[1], Elizabeth C. Martin[1], Sandip Kumar[2, 3], Jamie K. Hobbs[2], Matthew P. Johnson[1], Andrew Hitchcock[1] & C. Neil Hunter[1]

[1]School of Biosciences, University of Sheffield, Sheffield S10 2TN, United Kingdom

[2]Department of Physics and Astronomy, University of Sheffield, Sheffield S3 7HR, United Kingdom

[3]Department of Biochemistry, University of Oxford, Oxford OX1 3QU, United Kingdom

*Author for correspondence: c.vasilev@sheffield.ac.uk

**Abstract:** In the model purple phototrophic bacterium *Rhodobacter* (*Rba*.) *sphaeroides*, solar energy is converted via coupled electron and proton transfer reactions within the intracytoplasmic membranes (ICMs), infoldings of the cytoplasmic membrane that form spherical 'chromatophore' vesicles. These bacterial 'organelles' are ideal model systems for studying how the organisation of the photosynthetic complexes therein shape membrane architecture. In *Rba*. *sphaeroides*, light-harvesting 2 (LH2) complexes transfer absorbed excitation energy to dimeric reaction centre (RC)-LH1-PufX complexes. The PufX polypeptide creates a channel that allows the lipid soluble electron carrier quinol, produced by RC photochemistry, to diffuse to the cytochrome *bc*$_1$ complex, wherequinols are oxidised to quinones, with the liberated protons used to generate a transmembrane proton gradient and the electrons returned to the RC via cytochrome *c*$_2$. Proximity between cytochrome *bc*$_1$ and RC-LH1-PufX minimises quinone/quinol/cytochrome *c*$_2$ diffusion distances within this protein-crowded membrane, however this distance has not yet been measured. Here, we tag the RC and cytochrome *bc*$_1$ with yellow or cyan fluorescent proteins (Y/CFP) and record the lifetimes of YFP/CFP Förster resonance energy transfer (FRET) pairs in whole cells. FRET analysis shows that that these complexes lie on average within 6 nm of each other. Complementary high-resolution AFM of intact, purified chromatophores verifies the close association of cytochrome *bc*$_1$ complexes with RC-LH1-PufX dimers. Our results provide a structural basis for the close kinetic coupling observed by spectroscopy between RC-LH1-PufX and cytochrome *bc*$_1$, and explain how quinols/quinones and cytochrome *c*$_2$ shuttle on a millisecond timescale between these complexes, sustaining efficient photosynthetic electron flow.

**Keywords:** photosynthesis, purple bacteria, cytochrome $bc_1$, reaction centre, fluorescence-lifetime imaging microscopy (FLIM), atomic force microscopy (AFM).

**Abbreviations:** AFM, atomic force microscopy; CFP; cyan fluorescent protein; cyt, cytochrome; FLIM, fluorescence-lifetime imaging microscopy; FRET, Förster resonance energy transfer; ICM, intracytoplasmic membrane; LH, light-harvesting; PET, photosynthetic electron transfer; PMF, proton-motive force; *Rba*., *Rhodobacter*; RC, reaction centre; YFP, yellow fluorescent protein.

**Highlights:**

- *Rba. sphaeroides* produces intracytoplasmic membrane vesicles called chromatophores.
- Chromatophores are the site of cyclic electron flow between photosynthetic complexes.
- Rapid electron cycling requires close arrangement of the RC-LH1-PufX and cytochrome $bc_1$ complexes.
- Fluorescence lifetime measurements of tagged complexes reveals ~6 nm proximity.
- AFM of intact chromatophores confirms co-localisation of RC-LH1-PufX and cytochrome $bc_1$ complexes.

## 1 Introduction

Purple phototrophic bacteria grow photoheterotrophically under anaerobic conditions, generating ATP by anoxygenic photosynthesis [1], and contain an extensively invaginated intracytoplasmic membrane (ICM) system [2-5] that increases the internal surface area for absorbing and trapping solar energy. In the model purple bacterium *Rhodobacter* (*Rba.*) *sphaeroides* the photosynthetic pigment-protein complexes are embedded in vesicular ICMs, often referred to as 'chromatophores'. Excitation energy harvested by as many as 70 peripheral light-harvesting 2 (LH2) antenna complexes rapidly and efficiently migrates to ten or more dimeric reaction centre-light-harvesting 1-PufX (RC-LH1-PufX) 'core' complexes [6,7], with the LH2:RC stoichiometry governed by ambient light levels [8]. Charge separation at a RC ultimately reduces lipophilic quinones to quinols (for recent reviews see [9-12]. The quinols diffuse within the membrane and are oxidised by the cytochrome (cyt) $bc_1$ complex [13], which in turn reduces soluble cyt $c_2$ in the periplasm/chromatophore lumen. Reduced cyt $c_2$ migrates back to the RC and fills the electron hole, resetting the system for another light-powered charge separation.

61 Thus, repeated turnovers of this cyclic photosynthetic electron transfer (PET) chain generate a proton-
62 motive force (PMF), which is used to drive ATP production by the ATP synthase [14,15].

63 *Rba. sphaeroides* is also a model organism for studying the biogenesis of the ICM [3,16-18], and its
64 final architecture [3-6,8,19,20,21]. A combination of atomic force microscopy (AFM), electron
65 microscopy (EM), mass spectrometry, spectroscopy, and petascale computing has culminated in a 100
66 million-atom structural and functional model for all processes, from the absorption of light to
67 formation of ATP, and comprising 63–67 LH2 complexes, 13 RC–LH1–PufX complexes (11 dimers and
68 2 monomers), 4 cyt $bc_1$ dimers and 2 ATP synthases [6,15,22,23]. The number of cyt $bc_1$ complexes,
69 approximately four dimers per chromatophore, is limiting for the conversion of 'photons to ATP'
70 [6,15]. Depending on the level of light input, a chromatophore produces ATP at a rate between 82 and
71 158 $s^{-1}$, sustained by the rapid, back-and-forth shuttling of the soluble electron carrier cyt $c_2$, and of
72 the proton/electron carrier quinol/quinone, between the RC and the cyt $bc_1$ complex [15,23-26]. Such
73 rates of ATP synthesis are consistent with completion of cyclic electron flow, including turnovers of
74 the RC and the cyt $bc_1$ complexes, and diffusion of reduced/oxidised cyt $c_2$ and quinol/quinone
75 between them, within 20 ms. Given such constraints, the spatial arrangement of proteins in
76 bioenergetic membranes is important for efficient electron transport. In the case of chromatophore
77 membranes, the tight packing of complexes [15, 21, 23], required for rapid and efficient transfer of
78 excitation energy [7], could impair diffusion of quinol/quinone within the membrane bilayer, placing
79 constraints on the distance between RC and cyt $bc_1$ complexes [26]. Cartron *et al*. [6] provided
80 evidence that cyt $bc_1$ dimers and dimeric RC-LH1-PufX are found adjacent to each other in the
81 membranes but not necessarily in direct contact; His-tagged cyt $bc_1$ complexes were labelled with 5
82 nm-diameter Ni-NTA-Nanogold particles to facilitate AFM imaging [6], overcoming the lack of topology
83 of this complex on the outer face of chromatophore vesicles, apparent even in high-resolution AFM
84 conducted on whole membrane vesicles [21].

85 Given the importance of the relative positioning of RC-LH1-PufX and cyt $bc_1$ complexes for
86 chromatophore function, we used membrane-extrinsic protein tags to label RC-LH1-PufX and cyt $bc_1$
87 complexes, which confer new fluorescence properties for measuring inter-complex distances by
88 Förster resonance energy transfer (FRET). We constructed strains where RC-LH1-PufX and cyt $bc_1$ are
89 tagged with the FRET pair cyan fluorescent protein (CFP; FRET donor) and yellow fluorescent protein
90 (YFP; FRET acceptor), in both configurations. Fluorescence lifetimes of protein complexes labelled with
91 these fluorescent proteins were recorded in whole, live cells, showing that RC-LH1-PufX and cyt $bc_1$
92 complexes are within FRET distance and thus must reside close to one another, in agreement with our
93 earlier study utilising nanogold labelling. AFM of intact chromatophores, using the YFP tag to enhance

94 the topology of cyt $bc_1$ complexes, identified co-localised RC-LH1-PufX and cyt $bc_1$ complexes, sitting
95 at a distance compatible with the FRET measurements. These results confirm close spatial
96 arrangement of RC-LH1-PufX core complexes and cyt $bc_1$ dimers, further advancing our understanding
97 of the arrangement of the PET chain machinery in the ICM of purple bacteria.

98

99 **2 Materials and Methods**

100 **2.1 Growth of *Rba. sphaeroides***

101 Details of strains of *Rba. sphaeroides* used in this study are provided in Table 1. Wild-type and YFP/CFP-
102 tagged strains were grown at 34°C in M22+ medium [27]; 0.1% (w/v) casamino acids were added to
103 liquid cultures and plates were set with 1.5% (w/v) bacto-agar. Strains were stocked in LB medium
104 containing 50% (v/v) glycerol at −80°C.

105

106 **Table 1.** Strains of *Rba. sphaeroides* used in this study.

| Strain | Details | Source/reference |
|---|---|---|
| **Wild-type** | *Rba. sphaeroides* strain 2.4.1 | N/A |
| **cyt $bc_1$-CFP** | Fusion of CFP to the C-terminus of the cyt $bc_1$ cyt $c_1$ subunit | This study |
| **cyt $bc_1$-YFP** | Fusion of SYFP2 to the C-terminus of the cyt $bc_1$ cyt $c_1$ subunit | This study and [21] |
| **RC-CFP** | Fusion of CFP to the C-terminus of the RC-H subunit | [28] |
| **RC-YFP** | Fusion of SYFP2 to the C-terminus of the RC-H subunit | [28,29] |
| **cyt $bc_1$-CFP/RC-YFP** | Fusion of CFP to the C-terminus of the cyt $bc_1$ cyt $c_1$ subunit in the RC-YFP background | This study |

| | | |
|---|---|---|
| **RC-CFP/cyt *bc*$_1$-YFP** | Fusion of SYFP2 to the C-terminus of the cyt *bc*$_1$ cyt *c*$_1$ subunit in the RC-CFP background | This study |

107

108 **2.2 Generation of *Rba. sphaeroides* strains with tagged cytochrome *bc*$_1$ complexes**

109 The RC-YFP and RC-CFP strains have been described in our previous work [28,29]. In order to tag cyt
110 *bc*$_1$, the *syfp2* or *cfp* gene was fused to the 3´end of the *fbcC* gene (rsp_1394) by overlap extension
111 PCR. The PCR products were inserted into the pk18mob*sacB* plasmid by restriction cloning and the
112 resulting constructs were transferred from *E. coli* strain S17-1 into WT, RC-YFP or RC-CFP *Rba.*
113 *sphaeroides* (as appropriate – see Table 1) by conjugation. Transconjugants were selected on M22+
114 agar plates supplemented with 30 µg mL$^{-1}$ kanamycin and then grown in liquid culture with the same
115 concentration of kanamycin prior to serial dilution onto M22+ agar plates containing 10% (w/v)
116 sucrose to select second recombinants were the plasmid was excised, which was confirmed by replica
117 plating colonies on M22+ agar with sucrose in the presence and absence of kanamycin. Sucrose
118 resistant and kanamycin sensitive colonies were screened by colony PCR using primers that amplify
119 the *fbcC* locus and the flanking genomic region to confirm the presence of the fusion gene, which was
120 verified to be in-frame and have the correct sequence by automated DNA sequencing (Eurofins).

121 **2.3 UV/Vis/NIR spectroscopy**

122 Preparation of chromatophore membranes and determination of the RC-LH1-PufX, LH2 and cyt *bc*$_1$
123 concentrations have been described in detail previously [30]. Briefly, chromatophores were diluted to
124 an OD of 3.75 at 850 nm and spectra were collected between 350 and 1000 nm in a 4 mm path quartz
125 cuvette in a Cary 60 spectrophotometer (Agilent). The same sample was transferred to a 1 cm
126 disposable cuvette and spectra were collected before and after the addition of a few grains of sodium
127 dithionite. All spectra were normalised for a 1 cm path length, the RC-LH1-PufX and LH2 spectra were
128 deconvoluted as previously described [30] and the cyt *bc*$_1$ signal was obtained at 560 nm from the
129 dithionite-reduced minus air-oxidised difference spectrum.

130 **2.4 Photosynthetic growth curves**

131 Photosynthetic growth under anaerobic conditions was performed at room temperature in
132 completely full and sealed 17 mL sterile glass tubes inoculated from a semi-aerobically grown starter
133 culture to a starting optical density at 680 nm ($OD_{680}$) of ~0.05. Constant illumination at a light intensity
134 of ~50 µmol photons m$^{-2}$ s$^{-1}$ was provided by Osram 116 W Halogen bulbs and cultures were mixed

135 by agitation with sterile magnetic stir bars. Growth was measured by monitoring the $OD_{680}$ using a
136 WPA CO7000 Colorimeter.

137 **2.5 Fluorescence-lifetime imaging microscopy (FLIM)**

138 Fluorescence lifetime measurements were performed on our 'home-built' lifetime imaging
139 microscope equipped with an imaging spectrometer (Acton SP2558, Princeton Instruments) and a
140 single photon counting hybrid photodetector (HPM-100-50 Becker & Hickl), as described in detail in
141 Mothersole *et al*. [28]. Briefly, photosynthetically grown cells were spotted onto clear agarose gel pads
142 (1% w/v Agarose). Once the excess liquid was absorbed into the gel, the samples were sealed between
143 a microscope slide and a coverslip. Fluorescence lifetimes were recorded by parking the focused laser
144 spot over individual cells and collecting data for 0.2 s; measurements were performed on multiples
145 cells at 3–15 different locations on each sample. The fluorescence decay data was analysed with TRI2
146 FLIMfit software packages.

147 **2.6 AFM**

148 High-resolution AFM imaging of purified, intact *Rba. sphaeroides* chromatophores was performed as
149 described in detail in Kumar *et al*. [21]. Tapping mode imaging was performed in a buffered medium
150 using a Dimension FastScan AFM (Bruker).

151

152 **3 Results**

153 **3.1 Construction and characterisation of strains with fluorescently tagged cyt $bc_1$ complexes**

154 The CFP/YFP pair is suitable for assays of proximity based on excitation energy transfer from the CFP
155 donor to the YFP acceptor [31]. We have previously used this FRET pair in *Rba. sphaeroides* to
156 demonstrate the proximity of the RC-LH1-PufX complex to its assembly factor LhaA [28]. The strains
157 with the *syfp2* or *cfp* genes fused to the 3' end of *puhA*, which encodes the RC-H subunit, have been
158 described [28,29], and below we explain the construction of strains with the *syfp2* or *cfp* gene fused
159 to *fbcC*, which encodes the cyt $c_1$ subunit of the cyt $bc_1$ complex, including combinations of *puhA* and
160 *fbcC* fusions.

161 The cyt $c_1$ subunit of the cyt $bc_1$ complex tagged with a C-terminal 10×His-tag assembles into functional
162 cyt $bc_1$ dimers, and this strain has previously been used for nanogold-labelling of membranes and
163 affinity purification of cyt $bc_1$ [6,30]. This earlier work showed that the growth of the cyt $c_1$-$His_{10}$ strain
164 is very similar to the isogenic wild-type, so in principle there is no deleterious effect arising from

165 modification of the C-terminus of cyt $c_1$. Accordingly, we generated new allelic exchange plasmids that
166 replaced the His-tag sequence with the *syfp2* or *cfp* gene and integrated these constructs at the *fbcC*
167 (rsp_1394) locus in the genome of the WT to create the cyt $bc_1$-CFP and cyt $bc_1$-YFP strains, and into
168 the genomes of RC-YFP and RC-CFP strains to create the cyt $bc_1$-CFP/RC-YFP and the cyt $bc_1$-YFP/RC-
169 CFP strains. These manipulations generated a set of six markerless strains, four with single YFP or CFP
170 tags (RC-CFP, RC-YFP, cyt $bc_1$-CFP and cyt $bc_1$-YFP) and two dual-tagged strains (cyt $bc_1$-YFP/RC-CFP
171 and cyt $bc_1$-CFP/RC-YFP) (Table 1). Note that the cyt $bc_1$-YFP strain was introduced in our previous
172 publication [21] but its physiology was not characterised in that study, so it is reported here.

173 As levels of cyt $bc_1$ are limiting for ATP production [15], we first analysed growth of the YFP/CFP-tagged
174 strains to look for possible effects of tagging cyt $bc_1$ and combining this tag with the YFP/CFP-tagged
175 RC strains. The growth curves in Fig. 1A show that the strains with YFP/CFP-tagged cyt $bc_1$ all grew
176 photosynthetically at rates comparable to the WT (Fig. 1A). Reduced minus oxidised spectra (Fig. 1B)
177 were used to quantify the levels of cyt $bc_1$, which for all six markerless YFP/CFP-tagged strains were
178 comparable to the WT. The calculated ratios for RC: cyt $bc_1$ and RC: LH2 (Fig. 2C) show that the genomic
179 replacement strategy maintains the native photosystem stoichiometry. Thus, tagging the cyt $bc_1$
180 complex with YFP or CFP did not significantly alter the composition or function of the photosynthetic
181 apparatus.

182 **3.2 Proximity between cyt $bc_1$ and RC-LH1 complexes studied by FLIM**

183 Photosynthetically grown cells were spotted on an agarose gel and mounted on a standard microscope
184 slide with a coverslip to maintain the cells at near-physiological conditions. The samples were then
185 imaged using a home-built laser scanning confocal microscope that records a fluorescence emission
186 spectrum and lifetime for each pixel of the acquired image. The spectral response of the detectors
187 and the 0.1-10 ns time resolution makes this microscope particularly suitable for observing FRET
188 between fluorophores emitting and absorbing in the visible range, such as CFP and YFP.

189 Cells were excited at 420 nm and their emission was imaged through a 483/32 nm band-pass filter.
190 Examples of fluorescence images of cyt$bc_1$-CFP, RC-CFP and cyt$bc_1$-CFP/RC-YFP cells are shown in Fig.
191 2A, B, and C. In confocal imaging mode we were also able to acquire an emission spectrum from each
192 individual cell; Fig. 2D shows one such spectrum, the shape of which matches the CFP control. The
193 higher average fluorescence amplitude for cyt$bc_1$-CFP cells relative to RC-CFP (Fig. 2A, B, E) is in
194 apparent conflict with the higher levels of RCs in chromatophore membranes. Patches of non-
195 invaginated, respiratory cytoplasmic membranes present in photosynthetic cells [32] could contribute
196 to the CFP fluorescence, because these regions would contain cyt$bc_1$-CFP. Another contributory factor

197 is quenching of CFP fluorescence by proximity to the bacteriochlorophyll and carotenoid pigments in
198 the RC and LH1 complexes [29]. The bar chart in Fig. 2E displays the relative fluorescence amplitudes
199 for the three FP-tagged strains; the lowest average emission is from the cyt$bc_1$-CFP/RC-YFP strain so
200 the presence of RC-YFP partly quenches the fluorescence of cyt$bc_1$-CFP.

201
202
203
204
205
206
207
208
209
210
211
212
213
214
215
216
217
218
219
220
221
222
223

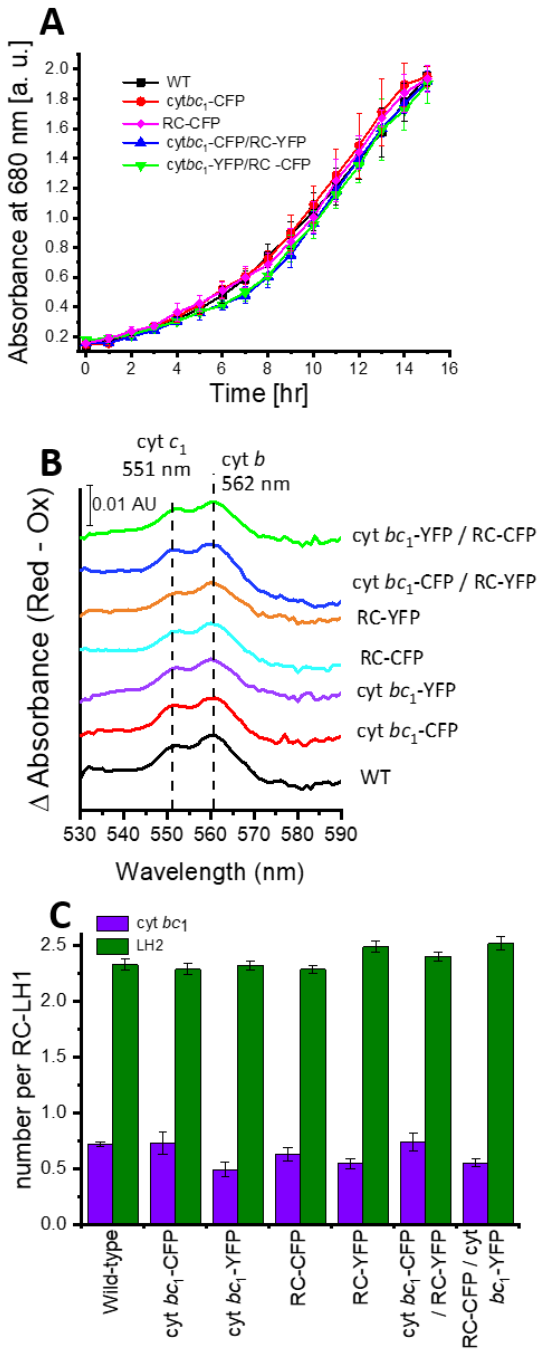


224 **Figure 1. Photosynthetic growth and complex stoichiometry of WT and FP-tagged strains. (A)** Growth
225 curves of WT (black), cyt $bc_1$-CFP (red), RC-CFP (magenta), and the two double mutants (blue and
226 green, respectively). Error bars indicate the standard deviation from the mean; $n$=3. **(B)** Dithionite-

227 reduced minus air-oxidised spectra used to quantify cyt $bc_1$ in all six strains, with respect to the WT.
228 **(C)** Calculated stoichiometric ratios for RC: cyt $bc_1$ and RC: LH2 for all the strains used in this work.

229

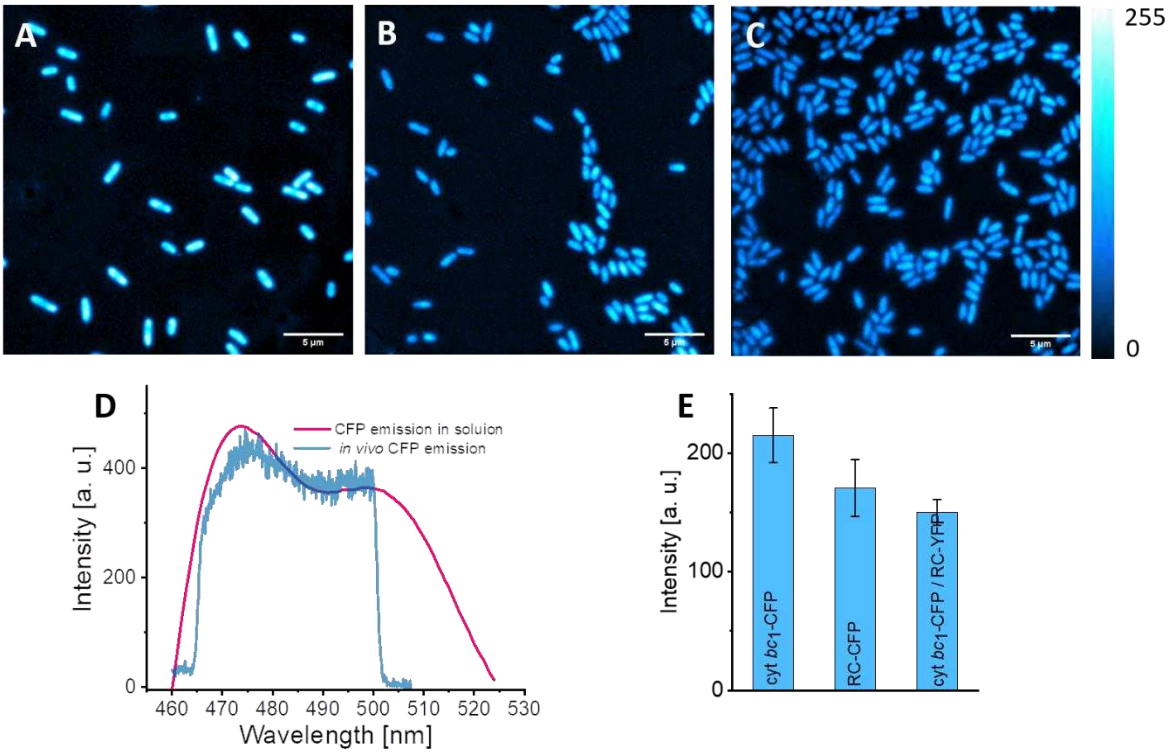


230

231 **Figure 2. Fluorescent lifetime imaging of live cells**. False colour fluorescent images of cyt$bc_1$-CFP cells
232 **(A)**, RC-CFP cells **(B)** and cyt$bc_1$-CFP/RC-YFP cells **(C)** immobilised on an agarose gel pad imaged
233 through 483/32 nm band-pass filter. **(D)** Fluorescence emission spectrum acquired from a single cell
234 (cyan) with an emission peak at 475 nm (the 483/32 nm band-pass filter cut-off is visible at 465 and
235 500 nm). A reference emission spectrum of CFP in solution is shown in red. **(E)** Relative fluorescence
236 amplitudes for 16 cells of each of the cyt$bc_1$-CFP, RC-CFP and cyt$bc_1$-CFP/RC-YFP strains.

237

238 To obtain a more quantitative estimate of cyt$bc_1$-YFP/CFP fluorescence quenching we recorded the
239 fluorescence lifetimes at 475 nm (peak emission of CFP) for cells of double-tagged strains containing
240 the cyt$bc_1$-YFP/RC -CFP and cyt$bc_1$-CFP/RC-YFP combinations and compared them with the RC-CFP and
241 cyt $bc_1$-CFP single mutant controls. FRET between CFP and YFP shortens the donor (CFP) fluorescence
242 lifetime, and the resulting decay curves are presented in Fig. 3. As expected from previous time-
243 resolved studies of CFP in mammalian and fungal cells [33-36], we observed a clear bi-exponential
244 decay for all four samples. The two intrinsic lifetime components likely originate from two different
245 conformations of the CFP chromophore [37,38] that can coexist and interchange on a millisecond

246 timescale (i.e., much slower than the fluorescence decay timescale). The best fit for the cyt*bc*$_1$-CFP
247 strain (Fig. 3A, violet) was achieved by using double-exponent decay function where the long-lived
248 component has an amplitude contribution $A_1$ = 0.24 ± 0.02 and lifetime $\tau_1$ = 2.96 ± 0.31 ns, while the
249 short-lived component has an amplitude contribution $A_2$ = 0.76 ± 0.02 and a lifetime $\tau_2$ = 0.74 ± 0.05
250 ns ($\chi_{red}^2$ = 1.03); all lifetimes and amplitudes are collated in Table 2. When a potential energy transfer
251 acceptor (YFP) is present in the cyt *bc*$_1$-CFP/RC-YFP double-tagged strain (Fig. 3A, green), the CFP
252 fluorescence lifetime decreases. The best fit for this decay curve is again a double-exponent decay
253 function, where the long-lived component has an amplitude contribution $A_1$ = 0.17 ± 0.03 and lifetime
254 $\tau_1$ = 2.24 ± 0.21 ns, and the second component has $A_2$ = 0.83 ± 0.18 and $\tau_2$ = 0.63 ± 0.04 ns.

255

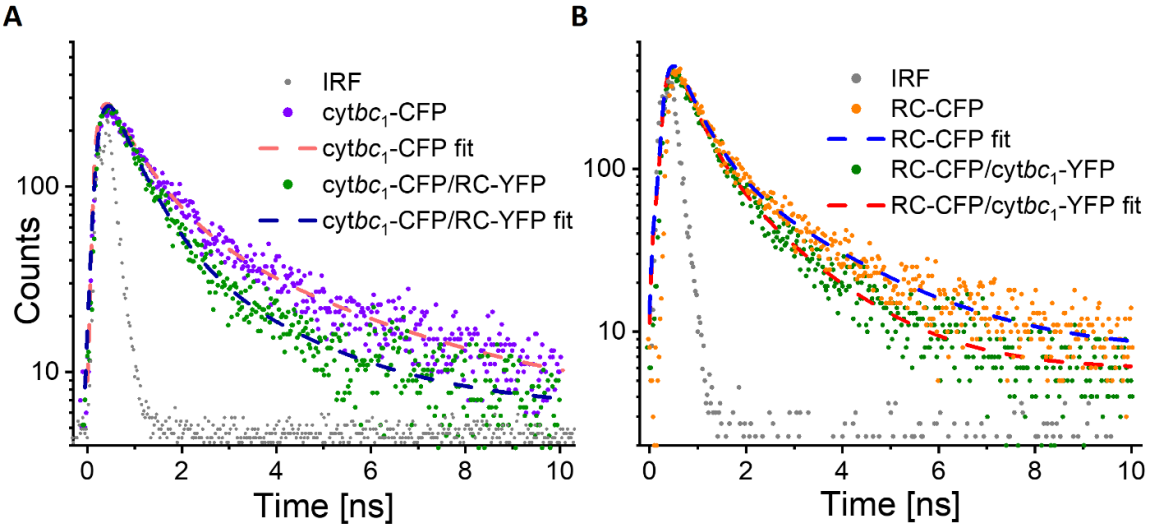


256 **Figure 3. Fluorescence decay curves for CFP tethered to cyt *bc*$_1$ or RC-LH1-PufX complexes, with or**
257 **without the YFP acceptor. (A)** Traces recorded on live cells containing cyt*bc*$_1$-CFP only (violet, best fit
258 shown with orange dashed line) and cells with excess of the acceptor fluorophore, containing cyt*bc*$_1$-
259 CFP plus RC-LH1-YFP (green, best fit shown with blue dashed line). The curves have been normalised
260 to the same maximum amplitude. The single mutant cells show double exponent decay with an
261 amplitude averaged lifetime of 1.27±0.1 ns, while the CFP amplitude averaged lifetime decreases to
262 0.89±0.05 ns for the double mutant. **(B)** Decay curves for live cells containing RC-LH1-CFP only (orange,
263 best fit shown with blue dashed line) and cells with excess of the donor fluorophore, containing RC-
264 LH1-CFP plus cyt*bc*$_1$-YFP (dark green, best fit shown with red dashed line). In this case, the CFP
265 amplitude averaged lifetime is 0.80±0.04 ns in single mutant cells, while the double mutant exhibits
266 an amplitude averaged lifetime of about 0.69±0.05 ns. The instrument response function (IRF) is
267 shown in grey.

268 When the positions of the donors and the acceptors were switched, with the CFP donor on the H-
269 subunit of the RC and the YFP acceptor on cyt *bc*$_1$, we used the RC-CFP strain as a control sample (Fig.
270 3B, orange data points). The best fit for the data in this case (Fig. 3B, blue dashed line) was achieved
271 using double-exponent decay function, where the long-lived component has an amplitude

contribution $A_1$ = 0.23 ± 0.04 and lifetime $\tau_1$ = 1.89 ± 0.1 ns, while the short-lived component has an amplitude contribution $A_2$ = 0.77 ± 0.04 and a lifetime $\tau_2$ = 0.48 ± 0.05 ns ($\chi_{red}^2$ = 1.04). With the cyt*bc*$_1$-YFP/RC-CFP combination in Fig. 3B, the CFP donor molecule on the RC H-subunit is likely in excess over the YFP acceptors on cyt *bc*$_1$, inverting the stoichiometry between the donors and acceptors relative to Fig. 3A. Thus, we observed an altered decay of CFP, and now the long-lived component, $A_1$ = 0.31 ± 0.04 and $\tau_1$ = 1.26 ± 0.16 ns, has a larger contribution and the short-lived component is less dominant (compared to the cyt *bc*$_1$-CFP/RC -YFP strain), with $A_2$ = 0.69 ± 0.02, with a lifetime of $\tau_2$ = 0.43 ± 0.05 ns ($\chi_{red}^2$ = 0.91); see also Table 2. In this configuration, some RC-CFP complexes are proximal to cyt *bc*$_1$-YFP acceptors, but the excess of RC-LH1-CFP donors over the cyt *bc*$_1$-YFP acceptors creates a large proportion of unquenched CFP donors which do not contribute to the FRET. This observation agrees with previously reported data for the CFP-YFP FRET pair [34-36]. It is worth noting that the CFP lifetimes in the two single-mutant strains differ significantly – the amplitude averaged lifetime for cyt *bc*$_1$-CFP single mutant is 1.27 ns, while the amplitude averaged lifetime for the RC-CFP single mutant is only 0.8 ns. As suggested above in relation to the fluorescence amplitudes in Fig. 2 the CFP lifetime is likely shortened by the proximity of the CFP, tethered to the RC-H subunit, to acceptor pigments in the RC-LH1 complex [28,29].

**Table 2**. Amplitudes and lifetimes from the FRET experiments with cyt *bc*$_1$ and the RC labelled with either CFP or YFP.

| Sample | $A_1$ | $\tau_1$ [ns] | $A_2$ | $\tau_2$ [ns] | $\tau_{av}$ [ns] | red. $\chi^2$ |
|---|---|---|---|---|---|---|
| **cyt *bc*$_1$-CFP** | 0.24±0.02 | 2.96±0.31 | 0.76±0.02 | 0.74±0.05 | 1.27±0.1 | 1.03 |
| **cyt *bc*$_1$-CFP/RC-YFP** | 0.17±0.03 | 2.24±0.21 | 0.83±0.18 | 0.63±0.04 | 0.89±0.05 | 1.096 |
| **RC-CFP** | 0.23±0.04 | 1.89±0.1 | 0.77±0.04 | 0.48±0.05 | 0.8±0.04 | 1.04 |
| **RC-CFP/cyt *bc*$_1$-YFP** | 0.31±0.04 | 1.26±0.16 | 0.69±0.02 | 0.43±0.05 | 0.69±0.05 | 0.91 |

The donor-acceptor energy transfer efficiency, *E*, can be calculated according to:

$$E = 1 - \frac{\tau_{DA}}{\tau_D}$$

294 where $\tau_D$ is the donor lifetime and $\tau_{DA}$ is the lifetime of the donor chromophore measured in the
295 presence of the acceptor. Based on the amplitude averaged lifetimes of the cyt $bc_1$-CFP sample, $\tau_{Dav}$ =
296 1.27 ns, and the cyt $bc_1$-CFP/RC-YFP sample, $\tau_{DAav}$ = 0.89 ns (Table 1), we calculate that the FRET
297 efficiency is around 30 %. The bulky nature of fluorescent proteins can prevent a close approach
298 between the chromophores, limiting FRET efficiencies to ~40 % [31]. In our experiments the proximity
299 between the two FRET markers is hindered further by the relatively large carrier membrane proteins;
300 in particular, the RC-LH1-PufX complex has overall lateral dimension of around 12 nm, which limits the
301 extent to which an FP tethered to the RC-H subunit could come within reach of a neighbouring cyt $bc_1$
302 complex.

303 The donor–acceptor distance, $r$, can be calculated using the measured efficiency and the Förster
304 distance, $R_0$, at which energy transfer efficiency is 50 %:

305 $$r = R_0 \left(\frac{1}{E} - 1\right)^{\frac{1}{6}}$$

306 $R_0$ for the CFP-YFP donor-acceptor pair is approximately 5.0 nm [39] and for E = 30 % we calculated a
307 donor-acceptor distance of approximately 5.8 nm. Taking into account this distance, together with the
308 relatively large dimension of the carrier proteins (cyt $bc_1$ has a lateral size of approximately 8.6 nm
309 while RC-LH1-PufX monomer is around 11 nm in diameter [40,41]), we can conclude that the carrier
310 proteins, RC-LH1 and cyt $bc_1$, are in very close proximity within the membrane.

311 **3.3 Proximity between cyt $bc_1$ and RC-LH1 complexes studied by AFM**

312 To corroborate the RC-LH1 to cyt $bc_1$ distance estimated from FRET, we collected high-resolution AFM
313 topographic data of intact chromatophores, purified from WT and cyt $bc_1$-YFP cells, using gentle
314 tapping imaging mode with optimized imaging conditions, as described previously [26]. In the paired
315 images for WT (Fig. 4A, C) and cyt$bc_1$-YFP (Fig. 4B, D) chromatophores the two upper panels show
316 coloured areas that indicate positions of LH2 (green), LH1, (red), RC (blue) and cyt $bc_1$ or cyt $bc_1$-YFP
317 (magenta) complexes. The lower panels (Fig 4C, D) show the positions of height profiles, which are
318 shown in panels E and F. For the RC-LH1-PufX dimer in WT chromatophores we measured a centre-to-
319 centre distance between RC H-subunits, of around 9.8-10.0 nm (Fig. 4A-F, blue lines). These numbers
320 are in good agreement with the existing structural model of the dimeric RC-LH1-PufX complex [40],
321 and AFM topographs of mature membranes of *Rba. sphaeroides* [3,26]. The RC-H subunits protrude
322 about 2.5 nm above the surrounding LH1 and LH2 protein.

323 We also identified a feature in the WT membrane approximately 12 nm from the RC-H subunit and
324 protruding 1 nm above the membrane surface (Fig. 4A, C, E, red lines), compatible with the expected

size and shape of a cyt $bc_1$ dimer [41]. Attachment of YFP to the periplasmic side of the cyt $bc_1$ complex would increase its surface topology by approximately 1.2 nm (Fig. 4F and G), in principle making it somewhat easier to image the cyt $bc_1$ dimer. Such a topological feature was found 12.8 nm from the RC-H subunit in a chromatophore purified from the cyt $bc_1$-YFP strain. (Fig. 4B, D, F, red lines). Fig. 4G places the known structures of the LH2 (green), LH1, (red), RC (blue) and cyt $bc_1$-YFP (magenta) complexes in the context of a curved membrane, showing the heights measured for the cytoplasmic faces of the complexes.

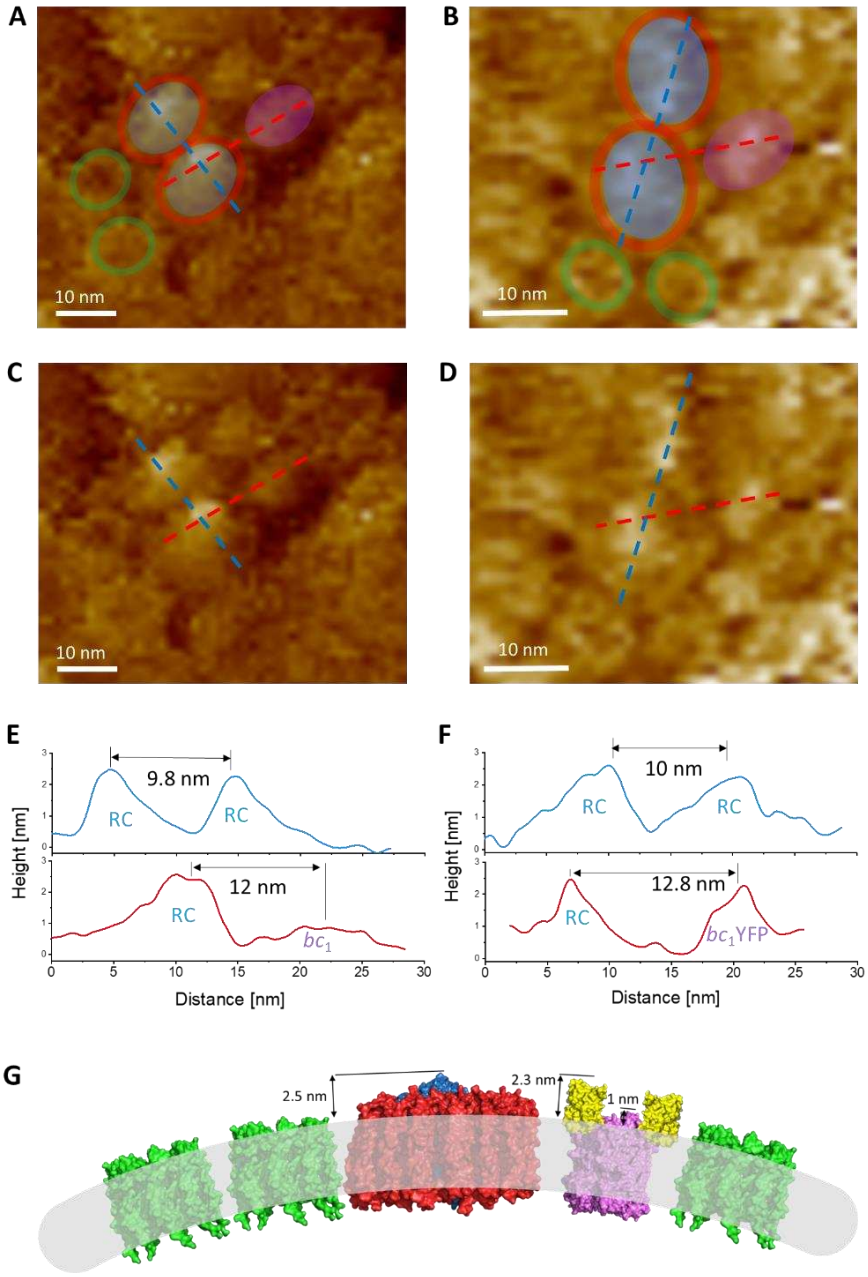


**Figure 4. High-resolution AFM topographic images of intact, purified WT and cyt$bc_1$-YFP chromatophores. (A)** Topography image of a WT membrane patch with coloured shapes to indicate

355 the positions of LH2 (green), LH1, (red), RC (blue) and cyt $bc_1$ (magenta) complexes. **(B)** Topography
356 image of a cyt$bc_1$-YFP membrane patch with coloured shapes to indicate complexes as in **(A)**. **(C, D)**
357 The same topography images as in **(A)** and **(B)** with cross-sections across an RC-LH1 dimer (blue dashed
358 line), and from an RC-LH1 to cyt $bc_1$ (**C**, red dashed line) or to cyt $bc_1$-YFP (**D**, red dashed line) pair of
359 dimers, and across RC-LH1 and cyt $bc_1$ (or cyt $bc_1$-YFP) nearest neighbours, respectively. **(E, F)** Height
360 profiles, corresponding to the cross-sections in panels **C** and **D**, respectively. The arrows indicate the
361 centre-to-centre distances between the protein complexes. **(G)** Schematic representation of the
362 arrangement of LH2 (green), RC-LH1 (red/blue), and cyt $bc_1$-YFP (magenta/yellow) proteins within the
363 ICM. Height protruding above the lipid bilayer is indicated with arrows.

364

365 **4 Discussion**

366 Estimating the distance between RC and cyt $bc_1$ complexes is important, given the crucial, rate-limiting
367 role played by cyt $bc_1$ complexes in the multistep conversion of absorbed light into a chemical form,
368 namely ATP [6,15]. Here we have used two different methods, based on FRET and membrane
369 topology, to verify the close proximity between RC and cyt $bc_1$ complexes in the photosynthetic
370 membranes of *Rba. sphaeroides*. We confined the measurements to whole cells to avoid the need for
371 fractionation into chromatophore vesicles, membrane growth sites, or cytoplasmic membranes
372 [32,42,43]. FRET analysis yielded an average distance of approximately 5.8 nm between RC- and
373 cyt$bc_1$- attached FRET partners, and AFM of whole vesicles gave values of 12 and 12.8 nm between
374 the RC-H subunit and cyt $bc_1$, or a cyt $bc_1$-attached YFP, respectively, at the convex cytoplasmic surface
375 of the chromatophore membrane. The membrane model in Fig. 5 emphasises the close proximity
376 between RC-LH1 and cyt $bc_1$ complexes, and it takes into account the sizes, typical stoichiometries and
377 distances of protein complexes within the chromatophore membrane.

378 Our finding of cyt $bc_1$ complexes adjacent to RCs has parallels with earlier work from the Daldal
379 laboratory on the closely related bacterium *Rba. capsulatus*. A series of papers characterised cyt $c_y$
380 that, in mutants lacking cyt $c_2$, still allowed phototrophic growth [44,45]. Cyt $c_y$ is tethered to the
381 membrane by an amino-terminal subdomain, with the membrane anchor and cytochrome separated
382 by a linker of approximately 70 residues. The fast kinetics of cyt $c_y$ oxidation by the RC, and re-
383 reduction by the cyt $bc_1$ complex [46], demonstrated the close proximity of RC and cyt $bc_1$ complexes,

384

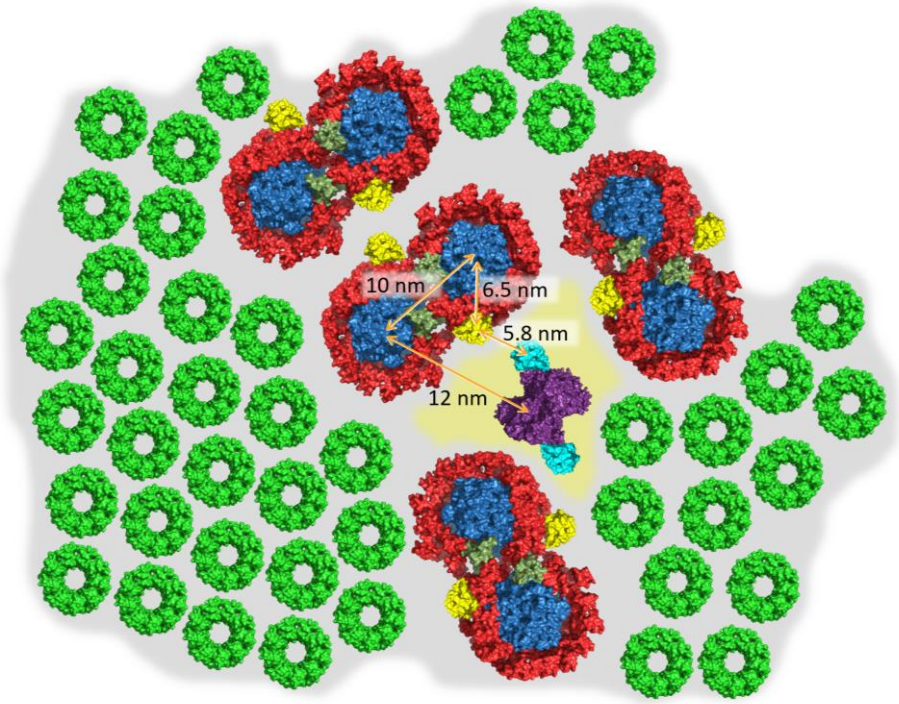


**Figure 5. Schematic representation of the chromatophore membrane of the cyt*bc*$_1$-CFP/RC-YFP double mutant, showing the stoichiometry and the relative distances between the label-carrying proteins, cyt *bc*$_1$ and RC-LH1.** The structures in yellow, protruding from the RC-LH1 dimers, are the YFP proteins attached to the C-terminus of the RC-H subunit. The complexes are embedded in a membrane (in grey), and the lipid and quinone-enriched environment surrounding the cyt *bc*$_1$ complex is shown in yellow.

and it was suggested that the long linker domain of cyt $c_y$ allows the cytochrome part of the protein to oscillate back and forth, sustaining cyclic electron transfer, and placing a 10 nm limit on the RC-to-cyt *bc*$_1$ distance [47]. A recent cryo-EM study of the respiratory cyt *bc*$_1$-*cbb*$_3$-type cyt *c* oxidase supercomplex of *Rba. capsulatus* shows the structural basis for cyt $c_y$ mediating electron transfers, in this case between the cyt *bc*$_1$ and *cbb*$_3$ components of this supercomplex [48]. Here, the transmembrane domain anchors the cytochrome domain of cyt $c_y$, confining it to a range of movements on the periplasmic surface of the *bc*$_1$-oxidase supercomplex, and allowing it to accept an electron from cyt $c_1$ and transfer it to cyt $c_{p2}$ on the *cbb*$_3$-type cyt *c* oxidase. If the same structural constraints apply to the RC-cyt *bc*$_1$ distance in *Rba. capsulatus*, and by extension to *Rba. sphaeroides*, then they are compatible with the model shown in Fig. 5, which illustrates the sizes of, and distances between, the three types of complex on view.

404 At the scale of a whole chromatophore, LH2 is the most abundant component, and closely packed
405 LH2-only domains are present [6, 15], which vary in size depending on the incident light intensity [8].
406 Modelling of energy conversion in a chromatophore vesicle from low-light grown cells [15] showed
407 that each RC becomes oxidised every 13–65 milliseconds, requiring repeated docking/undocking of
408 reduced/oxidised cyt $c_2$ at the RC surface [49-51], and also at the cyt $bc_1$ complex [52]. In addition,
409 there is concerted reduction of quinol at the RC $Q_B$ site, which must traverse the encircling LH1
410 complex, aided by conserved accessory quinone binding sites, and by PufX and protein-Y components
411 [53-55], and diffuse to the cyt $bc_1$ complex. Following oxidation at the cyt $bc_1$ complex [56,57],
412 quinones make the return journey to the RC $Q_B$ site, and the round trip is completed within 20 ms.
413 Given these time and therefore distance constraints it would clearly be advantageous to have cyt $bc_1$
414 complexes in the vicinity of RCs. Similar considerations apply to the photosystem II and cyt $b_6f$
415 complexes in the thylakoids of plants, at least at the level of diffusion of quinones between these
416 complexes [58, 59]. In Fig 5, the cyt $bc_1$ complex is shown sitting in a lipid and quinone-rich
417 nanodomain of the chromatophore membrane (yellow zone), as originally proposed by Comayras *et*
418 *al.* [60], and observed experimentally [6,30]. The current model for the chromatophore membrane
419 takes into account kinetic and structural data for all processes, from absorption of light to eventual
420 production of ATP [6,15,21-23]. In the present work we focused on the proximity between the RC-
421 LH1-PufX dimer and the cyt $bc_1$ complex, and Fig. 5 depicts a membrane nanodomain in which the cyt
422 $bc_1$ complex sits in a quinone pool that allows communication between this complex and up to six
423 reaction centres, with some RCs approaching within a few nanometres of the cyt $bc_1$ complex. Such
424 models (Fig. 5, and [60]) place each cyt $bc_1$ dimer close to a RC-LH1-PufX complex, but do not support
425 a single conformation of the RC-LH1-PufX dimer and the cyt $bc_1$ complex, and given that the cyt $bc_1$
426 complex sits in a lipid-enriched domain [30], a range of conformations is likely. Given the overall RC-
427 LH1: cyt $bc_1$ stoichiometry, some outlier RC-LH1-PufX complexes are likely to be situated more than 6
428 nm distant from a cyt $bc_1$. Such an arrangement could weaken the functional coupling between a few
429 RCs and cytochrome complexes; a population of more distal cyt $bc_1$ complexes might account for past
430 kinetic studies on *Rba. sphaeroides* conducted with variable concentrations of cyt $bc_1$ inhibitors, one
431 of which measured the rate of photooxidation of cyt $c_2$ [61], and another the kinetics of oxidation of
432 the RC acceptor $Q_A$ [62]. These studies reported some heterogeneity in electron transfer kinetics,
433 which was interpreted as evidence for two populations of RC-LH1 supercomplexes, some with a fixed
434 RC: $bc_1$ stoichiometry accompanied by a small population lacking cyt $bc_1$. [58, 61-63]. An alternative
435 explanation for such kinetic behaviour invoked heterogeneity in the membrane distribution of
436 electron transfer components [64]. However, this model assumes a random, disordered distribution
437 of complexes connected by the free diffusion of cyt $c_2$ and quinone, whereas there is some order in

438 the arrangement of complexes in *Rba. sphaeroides*, in the sense that LH2 and RC-LH1 complexes
439 segregate into domains [8,19-21, 65]. A comprehensive review of the functional coupling between RC-
440 LH1 and cyt $bc_1$ complexes by Lavergne *et al*. [26] suggested the possibility of a range of
441 supramolecular associations rather than a single strict stoichiometry. The model in Fig. 5 supports the
442 notion of quinone confinement [26, 58, 60] but our FRET and AFM data do not provide evidence for
443 the existence of a 'hardwired' RC-LH1-cyt $bc_1$ supercomplex, nor do they represent a random,
444 heterogeneous assortment of complexes. Our hypothesis is that cyt $bc_1$ complexes sit adjacent to, but
445 not necessarily in direct contact with, RC–LH1 complexes in a disordered fashion. Most likely, the
446 proximity between the complexes is instigated by the packing mismatch of the LH2 antenna complexes
447 and the RC–LH1 complexes within the chromatophore membrane [65].

448

449 **Author contributions:** C.V., J.K.H., M.P.J. and C.N.H. conceptualised and/or supervised the study. C.V.,
450 D.J.K.S., M.L.C., E.C.M., S.K. and A.H. performed the experiments and/or analysed the data. C.V.,
451 D.J.K.S., A.H. and C.N.H. wrote the paper.

452

453 **Acknowledgements:** C.N.H. and M.P.J. and gratefully acknowledge funding (BB/M000265/1,
454 BB/P002005/1 and BB/V006630/1) from the Biotechnology and Biological Sciences Research Council
455 UK. C.N.H. is also supported by European Research Council Synergy Award 854126. A.H. acknowledges
456 support from a Royal Society University Research Fellowship (award number URF\R1\191548).

457

458 **References**

459 [1] Hunter C.N., Daldal F., Thurnauer M.C. and Beatty J.T. (2009) The Purple Phototrophic Bacteria.
460 Advances in Photosynthesis and Respiration, Vol. 28, Springer, Dordrecht, The Netherlands.

461 [2] Konorty, M., Kahana, N., Linaroudis, A., Minsky, A., and Medalia, O. (2008) Structural analysis of
462 photosynthetic membranes by cryo-electron tomography of intact *Rhodopseudomonas viridis* cells. *J.*
463 *Struct. Biol.* 161**,** 393–400. **Doi:** 10.1016/j.jsb.2007.09.014.

464 [3] Tucker, J.D., Siebert, C.A., Escalante, M., Adams, P.G., Olsen, J.D., Otto, C., Stokes, D.L. and Hunter,
465 C.N. (2010) Membrane invagination in *Rhodobacter sphaeroides* is initiated at curved regions of the
466 cytoplasmic membrane, then forms both budded and fully detached spherical vesicles. *Mol. Microbiol.*
467 76, 833–847. **Doi:** 10.1111/j.1365-2958.2010.07153.x.

468 [4] Scheuring, S., Nevo, R., Liu, L.-N., Mangenot, S., Charuvi, D., Boudier, T., Prima, V., Hubert, P.,
469 Sturgis, J.N. and Reich, Z. (2014) The Architecture of *Rhodobacter sphaeroides* Chromatophores.
470 *Biochim. Biophys. Acta. Bioenerg*. 1837, 1263−1270. **Doi:** 10.1016/j.bbabio.2014.03.011.

471 [5] Noble, J.M., Lubieniecki, J., Savitzky, B.H., Plitzko, J., Engelhardt, H., Baumeister, W. and Kourkoutis,
472 L.F. (2018) Connectivity of centermost chromatophores in *Rhodobacter sphaeroides* bacteria. *Mol.*
473 *Microbiol.* 109, 812–825. **Doi:** 10.1111/mmi.14077.

474 [6] Cartron, M.L., Olsen, J.D., Sener, M., Jackson, P.J., Brindley, A.A., Qian, P., Dickman, M.J., Leggett,
475 G.J., Schulten, K. and Hunter, C.N. (2014) Integration of energy and electron transfer processes in the
476 photosynthetic membrane of *Rhodobacter sphaeroides. Biochim. Biophys. Acta.* 1837, 1769–1780.
477 **Doi:** 10.1016/j.bbabio.2014.02.003.

478 [7] Dahlberg, P.D., Ting, P.-C., Massey, S.C., Allodi, M.A., Martin, E.C., Hunter, C.N. and Engel, G.S.
479 (2017) Mapping the ultrafast flow of harvested solar energy in living photosynthetic cells. *Nat.*
480 *Commun.* 8, 988. **Doi:** 10.1038/s41467-017-01124-z.

481 [8] Adams, P.G. and Hunter, C.N. (2012) Adaptation of intracytoplasmic membranes to altered light
482 intensity in *Rhodobacter sphaeroides*. *Biochim Biophys. Acta.* 1817, 1616–1627. **Doi:**
483 10.1016/j.bbabio.2012.05.013.

484 [9] Mothersole, D.J., Farmer, D.A., Hitchcock, A. and Hunter, C.N. (2018). Photosynthetic apparatus in
485 purple bacteria. In *Light Harvesting in Photosynthesis*; Croce, R., van Grondelle, R., van Amerongen,
486 H., van Stokkum, I., (Eds.) (pp.95-120). CRC Press, USA. **Doi**: 10.1201/9781351242899.

487 [10] Gardiner, A.T., Nguyen-Phan, T.C and Cogdell, R.J. (2020) A comparative look at structural
488 variation among RC–LH1 'Core' complexes present in anoxygenic phototrophic bacteria. *Photosynth.*
489 *Res.* 145, 83-96. **Doi:** 10.1007/s11120-020-00758-3.

490 [11] Miller, L.C., Martin, D.S., Liu, L.N. and Canniffe, D.P. (2020) Composition, Organisation and
491 Function of Purple Photosynthetic Machinery. In: *Microbial Photosynthesis*; Wang, Q., (Eds.) (pp. 73-
492 114). Springer, Singapore. **Doi:** 10.1007/978-981-15-3110-1_4.

493 [12] Sarewicz, M., Pintscher, S., Pietras, R., Borek, A., Bujnowicz, Ł., Hanke, G., Cramer, W.A., Finazzi,
494 G. and Osyczka, A. (2021) Catalytic Reactions and Energy Conservation in the Cytochrome $bc_1$ and $b_6f$
495 Complexes of Energy-Transducing Membranes. *Chem. Rev.* 121, 2020-2108. **Doi:**
496 10.1021/acs.chemrev.0c00712.

[13] Crofts, A.R., Meinhardt, S.W., Jones, K.R. and Snozzi M. (1983) The role of the quinone pool in the cyclic electron-transfer chain of *Rhodopseudomonas sphaeroides*: a modified Q-cycle mechanism, *Biochim. Biophys. Acta.* 723, 202–218. **Doi:** 10.1016/0005-2728(83)90120-2.

[14] Feniouk, B.A. and Junge, W. (2009). Proton translocation and ATP synthesis by the FFATPase of purple bacteria. In: Hunter, C. N., Daldal, F., Thurnauer, M., Beatty, J. T. (Eds.) *The Purple Phototropic Bacteria*, p. 475–493. **Doi:** 10.1007/978-1-4020-8815-5_24.

[15] Sener, M., Strümpfer, J., Abhishek, S., Hunter, C.N. and Schulten, K. (2016) Overall energy conversion efficiency of a photosynthetic vesicle. *eLife* 5, e09541. **Doi:** 10.7554/eLife.09541.

[16] Pugh, R.J., McGlynn, P., Jones, M.R. and Hunter, C.N., (1998) The LH1–RC core complex of *Rhodobacter sphaeroides*: interaction between components, time-dependent assembly, and topology of the PufX protein. *Biochim. Biophys. Acta.* 1366, 301-316. **Doi**: 10.1016/S0005-2728(98)00131-5.

[17] Hunter, C.N., Tucker, J.D. and Niederman, R.A. (2005) The assembly and organisation of photosynthetic membranes in *Rhodobacter sphaeroides*. *Photochem. Photobiol. Sci*. 4, 1023-1027. **Doi:** 10.1039/B506099K.

[18] Koblízek, M., Shih, J.D., Breitbart, S.I., Ratcliffe, E.C., Kolber, Z.S., Hunter, C.N. and Niederman, R.A. (2005) Sequential assembly of photosynthetic units in *Rhodobacter sphaeroides* as revealed by fast repetition rate analysis of variable bacteriochlorophyll *a* fluorescence. *Biochim. Biophys. Acta* 1706, 220– 231. **Doi**: 10.1016/j.bbabio.2004.11.004.

[19] Bahatyrova, S., Frese, R.N., Siebert, C.A., Olsen, J.D., van der Werf, K.O., van Grondelle, R., Niederman, R.A., Bullough, P.A., Otto, C. and Hunter, C.N. (2004) The native architecture of a photosynthetic membrane. *Nature* 430, 1058-1061.

[20] Frese, R.N., Siebert, C.A., Niederman, R.A., Hunter, C.N., Otto, C. and van Grondelle, R. (2004) The long-range organization of a native photosynthetic membrane. *Proc. Natl. Acad. Sci. U. S. A*. 101, 17994-17999. **Doi:** 10.1073/pnas.0407295102.

[21] Kumar, S., Cartron, M.L., Mullin, N., Qian, P., Leggett, G.J., Hunter, C.N. and Hobbs, J.K. (2017) Direct Imaging of Protein Organization in an intact Bacterial Organelle Using High-Resolution Atomic Force Microscopy. *ACS Nano* 11, 126–133. **Doi:** 10.1021/acsnano.6b05647.

525 [22] Hitchcock, A., Hunter, C.N. and Sener, M. (2017) Determination of Cell Doubling Times from the
526 Return-on-Investment Time of Photosynthetic Vesicles Based on Atomic Detail Structural Models. *J.*
527 *Phys. Chem. B* 121, 3787-3797. **Doi:** 10.1021/acs.jpcb12335.

528 [23] Singharoy, A., Maffeo, C., Delgado-Magnero, K.H. Swainsbury, D.J.K., Sener, M., Kleinekathöfer,
529 U., Vant, J.E., Nguyen, J., Hitchcock, A., Isralewitz, B., Teo, I., Chandler, D., Stone, J., Phillips, J.,
530 Pogorelov, T.V., Mallus, M.I., Chipot,C., Luthey-Schulten, Z., Tieleman, P., Hunter, C.N., Tajkhorshid,
531 E., Aksimentiev, A. and Schulten, K. (2019) Atoms to Phenotypes: Molecular Design Principles of
532 Cellular Energy Metabolism. *Cell* 179, 1098-1111. **Doi:** 10.1016/j.cell.2019.10.021.

533 [24] Moser, C.C. and Dutton, P.L. (1988) Cytochrome *c* and $c_2$ binding dynamics and electron transfer
534 with photosynthetic reaction center protein and other integral membrane redox proteins.
535 *Biochemistry* 27, 2450–2246. **Doi**: 10.1021/bi00407a031.

536 [25] Gerencsér, L., Laczkó, G. and Maróti, P. (1999) Unbinding of oxidized cytochrome c from
537 photosynthetic reaction center of *Rhodobacter sphaeroides* is the bottleneck of fast turnover.
538 *Biochemistry* 38, 16866–16875. **Doi**: 10.1021/bi991563u.

539 [26] Lavergne, J., Verméglio, A. and Joliot, P. (2009) Functional coupling between reaction centers and
540 cytochrome $bc_1$ complexes. In Hunter, C. N., Daldal, F., Thurnauer, M., Beatty, J. T. (Eds.) *The Purple*
541 *Phototropic Bacteria*, p. 509–536, Springer, The Netherlands. **Doi**: 10.1007/978-1-4020-8815-5_26

542 [27] Hunter, C.N. & Turner, G. (1988) Transfer of Genes Coding for Apoproteins of Reaction Centre and
543 Light-harvesting LH1 Complexes to *Rhodobacter sphaeroides*. *J. Gen. Microbiol*. 134, 1471–1480. **Doi:**
544 10.1099/00221287-134-6-1471.

545 [28] Mothersole, D.J., Jackson, P.J., Vasilev, C., Tucker, J.D., Brindley, A.A., Dickman, M.J. and Hunter,
546 C.N. (2016) PucC and LhaA direct efficient assembly of the light-harvesting complexes in *Rhodobacter*
547 *sphaeroides*. *Mol. Microbiol.* 99, 307-327. **Doi:** 10.1111/mmi.13235.

548 [29] Grayson, K.J., Faries, K.M., Huang, X., Qian, P., Dilbeck, P., Martin, E.C., Hitchcock, A., Vasilev, C.,
549 Yuen, J.M., Niedzwiedzki, D.M., Leggett, G.J., Holten, D., Krimaeir, C. and Hunter, C.N. (2017)
550 Augmenting light coverage for photosynthesis through YFP-enhanced charge separation at the
551 *Rhodobacter sphaeroides* reaction centre. *Nat. Commun.* 8, 13972. **Doi:** 10.1038/ncomms13972.

552 [30] Swainsbury, D.J.K., Proctor, M.S., Hitchcock, A., Cartron, M.L., Qian, P., Martin, E.C., Jackson, P.J.,
553 Madsen, J., Armes, S.P. and Hunter, C.N. (2018) Probing the local lipid environment of the *Rhodobacter*
554 *sphaeroides* cytochrome $bc_1$ and *Synechocystis* sp. PCC 6803 cytochrome $b_6f$ complexes with styrene
555 maleic acid. *Biochim. Biophys. Acta. Bioenerg*. 1859, 215-225. **Doi:** 10.1016/j.bbabio.2017.12.005.

556 [31] Piston, D.W. & Kremers, G.J. (2007) Fluorescent protein FRET: the good, the bad and the ugly.
557 *Trends Biochem. Sci.* 32, 407–414. **Doi**: 10.1016/j.tibs.2007.08.003.

558 [32] Parks, L., and Niederman, R.A. (1978) Membranes of *Rhodopseudomonas sphaeroides* V.
559 Identification of bacteriochlorophyll *a*-depleted cytoplasmic membrane in phototrophically grown
560 cells. *Biochim. Biophys. Acta.* 511, 70–82. **Doi**: 10.1016/0005-2736(78)90065-2.

561 [33] Tramier, M., Gautier, I., Piolot, T., Ravalet, S., Kemnitz, K., Coppey, J., Durieux, C., Mignotte, V.
562 and Coppey-Moisan, M. (2002) Picosecond-hetero-FRET microscopy to probe protein-protein
563 interactions in live cells. *Biophys. J*. 83, 3570-3577. **Doi:** 10.1016/S0006-3495(02)75357-5.

564 [34] Becker, W., Bergmann, A., Hink, M.A., König, K., Benndorf, K. and Biskup, C. (2004) Fluorescence
565 lifetime imaging by time-correlated single-photon counting. *Microsc. Res. Tech*. 63, 58-66. **Doi:**
566 10.1002/jemt.10421.

567 [35] Duncan, R.R., Bergmann, A., Cousin, M.A., Apps, D.K. and Shipston, M.J. (2004) Multi-dimensional
568 time-correlated single photon counting (TCSPC) fluorescence lifetime imaging microscopy (FLIM) to
569 detect FRET in cells. *J. Microsc.* 215. 1-12. **Doi:** 10.1111/j.0022-2720.2004.01343.x.

570 [36] Millington, M., Grindlay, G.J., Altenbach, K., Neely, R.K., Kolch, W., Bencina, M., Read, N.D., Jones,
571 A.C., Dryden, D.T. and Magennis, S.W. (2007) High-precision FLIM-FRET in fixed and living cells reveals
572 heterogeneity in a simple CFP-YFP fusion protein. *Biophys. Chem*. 127, 155-164. **Doi:**
573 10.1016/j.bpc.2007.01.008.

574 [37] Seifert, M.H., Ksiazek, D., Azim, M.K., Smialowski, P., Budisa, N. & Holak, T.A. (2002) Slow
575 exchange in the chromophore of a green fluorescent protein variant. *J. Am. Chem. Soc*. 124, 7932–
576 7942. **Doi:** 10.1021/ja0257725.

577 [38] Bae, J.H., Rubini, M., Jung, G., Wiegand, G., Seifert, M.H.J., Azim, M.K., Kim, S.J., Zumbusch, A.,
578 Holak, T.A., Moroder, L. Huber, R. and Budisa, N. (2003) Expansion of the genetic code enables design
579 of a novel 'gold' class of green fluorescent proteins. *J. Mol. Biol.* 328, 1071–1081. **Doi:** 10.1016/s0022-
580 2836(03)00364-4.

581 [39] Tsien, R.Y. (1998) The green fluorescent protein. *Annu. Rev. Biochem*. 67, 509-544. **Doi:**
582 10.1146/annurev.biochem.67.1.509.

583 [40] Qian, P., Papiz, M.Z., Jackson, P.J., Brindley, A.A., Ng, I.W., Olsen, J.D., Dickman, M.J., Bullough,
584 P.A. & Hunter, C.N. (2013) Three-dimensional structure of the *Rhodobacter sphaeroides* RC-LH1-PufX

585 complex: dimerization and quinone channels promoted by PufX. *Biochemistry* 52, 7575-7585. **Doi:**
586 10.1021/bi4011946.

587 [41] Esser, L., Elberry, M., Zhou, F., Yu, C.A., Yu, L. and Xia D. (2007) Inhibitor-complexed structures of
588 the cytochrome $bc_1$ from the photosynthetic bacterium *Rhodobacter sphaeroides*. *J. Biol. Chem.* 283,
589 2846–2857. **Doi:** 10.1074/jbc.M708608200.

590 [42] Niederman, R.A., Mallon, D.E., and Langan, J.J. (1976) Membranes of *Rhodopseudomonas*
591 *sphaeroides*. IV. Assembly of chromatophores in low-aeration cell suspensions. *Biochim. Biophys.*
592 *Acta*. 440, 429–447. **Doi:** 10.1016/0005-2728(76)90076-1.

593 [43] Niederman, R.A., Mallon, D.E., and Parks, L.C. (1979) Membranes of *Rhodopseudomonas*
594 *sphaeroides*. VI. Isolation of a fraction enriched in newly synthesized bacteriochlorophyll *a*–protein
595 complexes. *Biochim. Biophys. Acta*. 555, 210–220. **Doi:** 10.1016/0005-2736(79)90161-5.

596 [44] Jenney Jr, F.E., and Daldal, F. (1993) A novel membrane-associated c-type cytochrome, cyt $c_y$, can
597 mediate the photosynthetic growth of *Rhodobacter capsulatus* and *Rhodobacter sphaeroides*. *EMBO*
598 *J*. 12, 1283-1292. **Doi:** 10.1002/j.1460-2075.1993.tb05773.x.

599 [45] Jenney Jr, F.E., Prince, R.C., and Daldal, F. (1994) Roles of the Soluble Cytochrome $c_2$ and
600 Membrane-Associated Cytochrome $c_y$ of *Rhodobacter capsulatus* in Photosynthetic Electron Transfer.
601 *Biochemistry* 33, 2496-2502. **Doi:** 10.1021/bi00175a019.

602 [46] Myllykallio, H., Drepper, F., Mathis, P. and Daldal, F. (1998) Membrane-Anchored Cytochrome $c_y$
603 Mediated Microsecond Time Range Electron Transfer from the Cytochrome $bc_1$ Complex to the
604 Reaction Center in *Rhodobacter capsulatus*. *Biochemistry* 37, 5501-5510. **Doi:** 10.1021/bi973123d.

605 [47] Lee, D.W., Öztürk, Y., Osyczka, A., Cooley, J.W. and Daldal, F. (2008). Cytochrome $bc_1$-$c_y$ fusion
606 complexes reveal the distance constraints for functional electron transfer between photosynthesis
607 components. *J. Biol. Chem*. 283, 13973-13982. **Doi:** 10.1074/jbc.M800091200.

608 [48] Steimle, S., van Eeuwen ,T,. Ozturk, Y., Kim, H.J., Braitbard, M., Selamoglu, N., Garcia, B.A.,
609 Schneidman-Duhovny, D., Murakami, K. and Daldal, F. (2021) Cryo-EM structures of engineered active
610 $bc_1$-$cbb_3$ type $CIII_2CIV$ super-complexes and electronic communication between the complexes. *Nat.*
611 *Commun.* 12, 929. **Doi:** 10.1038/s41467-021-21051-4.

612 [49] Autenrieth, F., Tajkhorshid, E., Schulten, K. and Luthey-Schulten, Z. (2004) Role of water in
613 transient cytochrome $c_2$ docking. *J. Phys. Chem. B*. 108, 20376–20387. **Doi:** 10.1021/jp047994q.

614 [50] Vasilev, C., Brindley, A.A., Olsen, J.D., Saer, R.G., Beatty, J.T. and Hunter, C.N. (2014) Nano-
615 mechanical mapping of the interactions between surface-bound RC-LH1-PufX core complexes and
616 cytochrome $c_2$ attached to an AFM probe. *Photosynth. Res*. 120, 169-180. **Doi:** 10.1007/s11120-013-
617 9812-7.

618 [51] Vasilev, C., Mayneord, G.E., Brindley, A.A., Johnson, M.P. and Hunter, C.N. (2019) Dissecting the
619 cytochrome $c_2$-reaction centre interaction in bacterial photosynthesis using single molecule force
620 spectroscopy. *Biochem. J.* 476, 2173-2190. **Doi:** 10.1042/BCJ20170519.

621 [52] Singharoy, A., Barragan, A.M., Thangapandian, S., Tajkhorshid, E. and Schulten, K. (2016) Binding
622 site recognition and docking dynamics of a single electron transport protein: cytochrome $c_2$. *J. Am.*
623 *Chem. Soc*. 138, 12077–12089. **Doi:** 10.1021/jacs.6b01193.

624 [53] Swainsbury, D.J.K., Qian, P., Jackson, P.J., Faries, K.M., Niedzwiedzki, D.M., Martin, E.C., Farmer,
625 D.A., Malone, L.A., Thompson, R.F., Ranson, N.A., Canniffe, D.P., Dickman, M.J., Holten, D., Kirmaier,
626 C., Hitchcock, A. and Hunter, C.N. (2021) Structures of *Rhodopseudomonas palustris* RC-LH1
627 complexes with open or closed quinone channels. *Sci. Adv.* 7, eabe2631. **Doi:** 10.1126/sciadv.abe2631.

628 [54] Qian, P., Swainsbury, D.J.K., Croll, T.I., Salisbury, J.H., Martin, E.C., Jackson, P.J., Hitchcock, A.,
629 Castro-Hartmann, P., Sader, K., and Hunter, C.N., (2021) Cryo-EM structure of the *Rhodobacter*
630 *sphaeroides* RC-LH1 core monomer complex at 2.5 Å. *Biochem. J.* 478, 3775–3790. **Doi:**
631 10.1042/BCJ20210631.

632 [55] Qian, P., Swainsbury, D.J.K., Croll, T.I., Salisbury, J.H., Martin, E.C., Jackson, P.J., Hitchcock, A.,
633 Castro-Hartmann, P., Sader, K., and Hunter, C.N., (2021) Cryo-EM structure of the *Rhodobacter*
634 *sphaeroides* RC-LH1 core dimer complex at 2.9 Å. *Biochem. J.* In press. **Doi**: 10.1042/BCJ20210696.

635 [56] Crofts, A.R. (2004) The cytochrome $bc_1$ complex: function in the context of structure. *Ann. Rev.*
636 *Physiol*. 66, 689–733. **Doi:** 10.1146/annurev.physiol.66.032102.150251.

637 [57] Crofts, A.R., Lhee, S., Crofts, S.B., Cheng, J. and Rose, S. (2006) Proton pumping in the $bc_1$ complex:
638 A new gating mechanism that prevents short circuits. *Biochim. Biophys. Acta.* 1757, 1019–1034. **Doi:**
639 10.1016/j.bbabio.2006.02.009.

640 [58] Lavergne, J. and Joliot, P. Restricted diffusion in photosynthetic membranes, *Trends Biochem. Sci.*
641 16 (1991) 129-134.

642 [59] Johnson, M.P., Vasilev, C., Olsen, J.D., and Hunter, C.N. (2014) Nanodomains of cytochrome $b_6f$
643 and photosystem II complexes in plant photosynthetic membranes. *Plant Cell* 26, 3051-3061. **Doi:**
644 10.1105/tpc.114.127233.

645 [60] Comayras F, Jungas C, Lavergne J. (2005) Functional consequences of the organization of the
646 photosynthetic apparatus in *Rhodobacter sphaeroides*. I. Quinone domains and excitation transfer in
647 chromatophores and reaction center antenna complexes. *J. Biol Chem.* 280, 11203-11213. **Doi:**
648 10.1074/jbc.M412088200.

649 [61] Verméglio, A., Joliot, P. and Joliot, A. (1993) The rate of cytochrome $c_2$ photooxidation reflects the
650 subcellular distribution of reaction centers in *Rhodobacter sphaeroides* Ga cells, *Biochim. Biophys.*
651 *Acta.* 1183, 352-360. **Doi**: 10.1016/0005-2728(93)90239-c.

652 [62] Joliot, P., Joliot, A. and Verméglio, A. (2005) Fast oxidation of the primary electron acceptor under
653 anaerobic conditions requires the organization of the photosynthetic chain of *Rhodobacter*
654 *sphaeroides* in supercomplexes, *Biochim. Biophys. Acta.* 1706, 204-214. **Doi**:
655 10.1016/j.bbabio.2004.11.002.

656 [63] Joliot, P., A. Verméglio, A. Joliot, A., (1989) Evidence for supercomplexes between reaction
657 centers, cytochrome $c_2$ and cytochrome $bc_1$ complex in *Rhodobacter sphaeroides* whole cells, *Biochim.*
658 *Biophys. Acta.* 975, 336-345. **Doi**: 10.1016/S0005-2728(89)80341-X.

659 [64] Crofts, A., Guergova-Kuras, M., Hong, S. (1998) Chromatophore heterogeneity explains
660 phenomena seen in *Rhodobacter sphaeroides* previously attributed to supercomplexes. *Photosynth.*
661 *Res.* 55, 357-362. **Doi**: 10.1023/A:1005940120396.

662 [65] Frese, R.N., Pàmies, J.C., Olsen, J.D., Bahatyrova, S., van der Weij-de Wit, C.D., Aartsma, T.J., Otto,
663 C., Hunter, C.N., Frenkel, D., and van Grondelle, R. (2008) Protein shape and crowding drive domain
664 formation and curvature in biological membranes. *Biophys. J.* 19, 640-647. **Doi**:
665 10.1529/biophysj.107.116913.

666